2017 IEEE Conference on Control Technology and Applications (CCTA)
August 27-30, 2017. Kohala Coast, Hawai'i, USA

Central Safety Factor Control in DIII-D using Neutral Beam Injection and Electron Cyclotron Launchers in Zero Input-Torque Scenarios

Andres Pajares and Eugenio Schuster

Abstract— **The tokamak is a torus-shaped machine whose final purpose is generating energy from nuclear fusion reactions. In order to achieve this goal, a reactant plasma is confined inside the tokamak by means of magnetic fields. For a tokamak to be commercially competitive, operation for long periods of time at high-performance operating points will be needed. Those high-performance scenarios are characterized by a steady-state, stable plasma operation in which the safety factor, a property of the plasma that measures the pitch of the magnetic field lines, plays a decisive role. In particular, control of the central safety factor, which is the value of the safety factor at the tokamak magnetic axis, is one of the crucial aspects to the success of tokamak devices due to its close relationship to magneto-hydrodynamic stability. Therefore, control algorithms for the central safety factor in tokamaks will be required. In the present work, a linear controller is proposed for the regulation of the central safety factor using neutral beam injection and electron cyclotron launchers. This controller is designed to guarantee a zero input torque delivered by the neutral beam injection system. The controller performance is tested via a simulation study in a DIII-D scenario.**

I. Introduction

Nowadays, the tokamak is one of the most promising devices to obtain energy by means of nuclear fusion. It is a torus-shaped device in which a gas, typically a mix of hydrogen isotopes like deuterium and tritium, is injected. This gas is heated to very high temperatures ($\sim$ 10 million degrees) in order to overcome the Coulombic repulsion force that exists between its particles and obtain energy from nuclear fusion reactions. Due to such high temperature, the gas is normally in plasma state, where ions and electrons are dissociated. The fact that electrons and ions are separated in a plasma provides it with very special characteristics, such as the capability to drive electrical current and be confined inside a particular volume by means of magnetic fields. These characteristics motivated the creation and development of magnetic confinement devices, the category in which tokamaks are included [1]. A plasma magnitude that is of crucial importance for stability and performance in tokamaks is the so-called safety factor, q, which is a measure of the pitch of the magnetic field lines. In particular, the limit $q \geq 1$ is of special relevance due to its close relationship with the triggering of certain magneto-hydrodynamic (MHD) instabilities [1]. Such MHD instabilities substantially decrease fusion performance and may terminate the confined plasma. For monotonically increasing safety-factor profiles, q achieves a minimum on the magnetic axis of the tokamak (see Fig. 1). Therefore, control of q at the magnetic axis (also known as central safety factor, q_0) is key for the success of tokamaks as efficient means of producing energy.

Intensive work has been carried out to find control algorithms for the q profile and/or q_0. Control of the q profile was experimentally demonstrated in both low and high plasma-confinement scenarios in the DIII-D tokamak [2], [3], [4], [5]. This previous work based the control design on a nonlinear, physics-based, control-oriented model of the plasma dynamics [6]. Other previous work proposed q profile and/or q_0 controllers for tokamaks different from DIII-D like, for example, NSTX-U [7], [8], JET [9] or ITER [10], the next-generation tokamak currently under construction. Some of the actuators used for q or q_0 control in previous work are plasma current modulation, auxiliary power modulation, density control, and plasma shape modification.

A particular tokamak scenario that is of special interest in current magnetic-control research is that one in which the injected auxiliary power produces an close-to-zero input torque. These scenarios, known as zero input-torque scenarios, will most likely be found in future burning-plasma tokamaks such as ITER [11]. Also, tokamaks working with zero input torque are more susceptible to suffer locked modes, a particular type of MHD instability, due to low plasma rotation [11]. Therefore, controllers that can ensure q_0 regulation under zero input-torque constraints are presently required for physics studies. In this work, a proportional-integral-derivative (PID) q_0 controller for zero input-torque, high-performance scenarios is presented. A nonlinear, physics-based, control-oriented modeling approach is employed. The control-oriented model is generated using DIII-D data from TRANSP [12], a tokamak plasma-transport simulation code widely used within the fusion community. The actuation method used by the controller is auxiliary power modulation by means of neutral beam injectors (NBI's), which are configured to produce zero input-torque, and electron cyclotron (EC) launchers. The zero input-torque configuration adds significant constraints to the control scheme. These constraints decrease the existent actuation capability over q_0, and evidently increase the complexity of the control problem.

This work is organized as follows. The nonlinear model for the q_0 evolution is introduced in Section II. The nonlinear model is discretized using finite differences and linearized in Section III. The PID control design is detailed in Section IV, together with the characterization of the zero input-torque condition. A simulation study is presented in Section V to illustrate the controller performance. Finally, a summary and possible future work are presented in Section VI.

This work was supported in part by the U.S. Department of Energy (DE-SC0010661). A. Pajares (andres.pajares@lehigh.edu) and E. Schuster are with the Department of Mechanical Engineering and Mechanics, Lehigh University, Bethlehem, PA 18015, USA.

II. Central Safety Factor Evolution Model

Magnetic field lines are normally closed in tokamaks and guide the particles in helical paths as shown in Fig. 1. The magnetic field, $\bar{B}$, is expressed as the summation of two components, $\bar{B} = \bar{B}_\phi + \bar{B}_\theta$, where $\bar{B}_\phi$ is the toroidal magnetic field and $\bar{B}_\theta$ is the poloidal magnetic field. The poloidal magnetic flux is defined by $\Psi = \int_S \bar{B}_\theta \cdot d\bar{S}$, where S is the surface bounded by the toroidal ring passing through each point P as depicted in Fig. 1. Points of equal poloidal magnetic flux Ψ define nested magnetic-flux surfaces. An axisymmetric disposition of the magnetic-flux surfaces around the so-called magnetic axis, as shown in Fig. 2, is normally found in tokamaks if ideal MHD conditions are assumed. Under such assumption, a one-dimensional model in the spatial domain can be used. The mean effective minor radius, ρ, is the magnitude used to index the magnetic-flux surfaces, and it is related to the toroidal magnetic flux, Φ, and to the vacuum toroidal magnetic field at the geometric major radius R_0 of the tokamak, $B_{\phi,0}$, by means of $\pi B_{\phi,0}\rho^2 = \Phi$. The mean effective minor radius is normalized as $\hat{\rho} = \rho/\rho_\mathrm{b}$, where ρ_b is the value of ρ at the last closed magnetic-flux surface as depicted in Fig. 2. The non-dimensional variable $\hat{\rho}$ is the spatial coordinate used in this one-dimensional model. The q profile is related to both Φ and Ψ, and is defined as

$$q(\hat{\rho},t) = \frac{d\Phi}{d\Psi} = -\frac{d\Phi}{2\pi d\psi} = -\frac{B_{\phi,0}\rho_\mathrm{b}^2\hat{\rho}}{\partial\psi/\partial\hat{\rho}}, \tag{1}$$

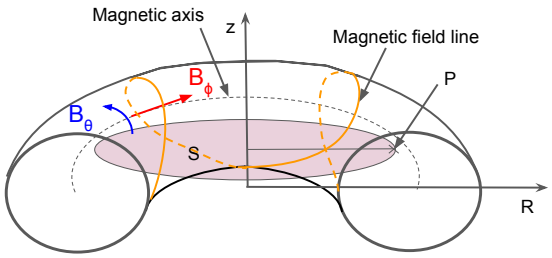

Fig. 1. Helical magnetic field lines in the tokamak define a poloidal magnetic flux through the surface S associated with the point P.

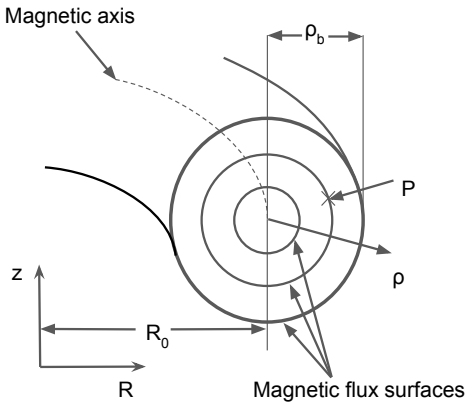

Fig. 2. Magnetic flux surfaces in a tokamak. Each magnetic flux surface is characterized by a constant poloidal magnetic flux Ψ.

where t is the time and $\psi(\hat{\rho},t)$ is the poloidal stream function, $\Psi = 2\pi\psi$. The central safety factor, $q_0(t)$, is given by

$$q_0(t) = q(\hat{\rho}=0) = -\left.\frac{B_{\phi,0}\rho_\mathrm{b}^2\hat{\rho}}{\partial\psi/\partial\hat{\rho}}\right|_{\hat{\rho}=0}. \tag{2}$$

The evolution of ψ is described by the magnetic diffusion equation [13],

$$\frac{\partial\psi}{\partial t} = \frac{\eta(T_\mathrm{e})}{\mu_0\rho_\mathrm{b}^2\hat{F}^2}\frac{1}{\hat{\rho}}\frac{\partial}{\partial\hat{\rho}}\left(\hat{\rho}D_\psi\frac{\partial\psi}{\partial\hat{\rho}}\right) + R_0\hat{H}\eta(T_\mathrm{e})j_\mathrm{ni}, \tag{3}$$

where $\eta(T_\mathrm{e})$ is the plasma resistivity, $T_\mathrm{e}(\hat{\rho},t)$ is the electron temperature, μ_0 is the vacuum permeability, $D_\psi(\hat{\rho}) = \hat{F}(\hat{\rho})\hat{G}(\hat{\rho})\hat{H}(\hat{\rho})$, where $\hat{F}$, $\hat{G}$, and $\hat{H}$ are spatially varying geometric factors pertaining to the magnetic configuration of a particular plasma equilibrium [14], and j_ni is the non-inductive current density. The boundary conditions are given by

$$\left.\frac{\partial\psi}{\partial\hat{\rho}}\right|_{\hat{\rho}=0} = 0, \quad \left.\frac{\partial\psi}{\partial\hat{\rho}}\right|_{\hat{\rho}=1} = -\frac{\mu_0}{2\pi}\frac{R_0}{\hat{G}|_{\hat{\rho}=1}\hat{H}|_{\hat{\rho}=1}}I_\mathrm{p}(t), \tag{4}$$

where $I_\mathrm{p}(t)$ is the total plasma current.

Control-oriented models for the electron temperature, electron density, plasma resistivity, and non-inductive current density are used [6]. The electron temperature, $T_\mathrm{e}(\hat{\rho},t)$, is given by

$$T_\mathrm{e}(\hat{\rho},t) = T_\mathrm{e}^\mathrm{prof}(\hat{\rho})I_\mathrm{p}(t)^\gamma P_\mathrm{tot}(t)^\epsilon n_\mathrm{e}(t)^\zeta, \tag{5}$$

where $T_\mathrm{e}^\mathrm{prof}(\hat{\rho})$ is a reference profile, $P_\mathrm{tot}(t)$ is the total power injected to the plasma, $n_\mathrm{e}(t)$ is the electron density, and the parameters γ, ϵ and ζ are constants that describe how the plasma temperature scales with $I_\mathrm{p}(t)$, $P_\mathrm{tot}(t)$ and $n_\mathrm{e}(t)$.

The electron density, $n_\mathrm{e}(\hat{\rho},t)$, is modeled as

$$n_\mathrm{e}(\hat{\rho},t) = n_\mathrm{e}^\mathrm{prof}(\hat{\rho})\bar{n}_\mathrm{e}(t), \tag{6}$$

where $n_\mathrm{e}^\mathrm{prof}(\hat{\rho})$ is a reference profile, and $\bar{n}_\mathrm{e}(t)$ is the line-averaged electron density, which is defined as $\bar{n}_\mathrm{e}(t) = \int_0^1 n_\mathrm{e}(\hat{\rho},t)d\hat{\rho}$.

The plasma resistivity $\eta(T_\mathrm{e})$ is given by

$$\eta(\hat{\rho},t) = \frac{k_\mathrm{sp}(\hat{\rho})Z_\mathrm{eff}}{T_\mathrm{e}^{3/2}(\hat{\rho},t)}, \tag{7}$$

where $k_\mathrm{sp}(\hat{\rho})$ is a constant reference profile, and Z_eff is the average charge of the ions in the plasma, which is assumed constant in this model.

Two sources of non-inductive current density are considered: the self-generated bootstrap current, and the current density externally injected by auxiliary sources. In this work, NBI and EC launchers are the auxiliary sources employed for current-drive purposes. Therefore, j_ni can be expressed as

$$j_\mathrm{ni}(\hat{\rho},t) = \sum_{i=1}^{N_\mathrm{NB}} j_{\mathrm{NB},i}(\hat{\rho},t) + j_\mathrm{EC}(\hat{\rho},t) + j_\mathrm{BS}(\hat{\rho},t), \tag{8}$$

where $j_{\mathrm{NB},i}$ is the non-inductive current density generated by the i-th NBI, N_NB is the total number of NBI's available in

the tokamak, j_{EC} is the non-inductive current density generated by the EC launchers, and j_{BS} is the non-inductive current density produced by the bootstrap effect. For the NBI's, the non-inductive current density contribution is modeled as

$$j_{\text{NB},i}(\hat{\rho},t) = j_{\text{NB},i}^{\text{prof}}(\hat{\rho})\frac{T_{\text{e}}(\hat{\rho},t)^{\delta_{\text{NB},i}}}{n_{\text{e}}(\hat{\rho},t)}P_{\text{NB},i}(t), \tag{9}$$

where $j_{\text{NB},i}^{\text{prof}}(\hat{\rho})$ is a reference deposition profile for the i-th NBI, $\delta_{\text{NB},i}$ is a constant related to the current-drive efficiency of the i-th NBI, and $P_{\text{NB},i}(t)$ is the injected power associated to the i-th NBI. Similarly, the EC current density contribution is modeled as

$$j_{\text{EC}}(\hat{\rho},t) = j_{\text{EC}}^{\text{prof}}(\hat{\rho})\frac{T_{\text{e}}(\hat{\rho},t)^{\delta_{\text{EC}}}}{n_{\text{e}}(\hat{\rho},t)}P_{\text{EC}}(t), \tag{10}$$

where $j_{\text{EC}}^{\text{prof}}(\hat{\rho})$ is a reference deposition profile, and $P_{\text{EC}}(t)$ is the EC injected power. The bootstrap current contribution is modeled in this work as [15]

$$j_{\text{BS}}(\hat{\rho},t) = \frac{R_0}{\hat{F}(\hat{\rho})}\left(\frac{\partial\psi}{\partial\hat{\rho}}\right)^{-1}\big[2\mathcal{L}_{31}(\hat{\rho})T_{\text{e}}(\hat{\rho},t)\frac{\partial n_{\text{e}}(\hat{\rho},t)}{\partial\hat{\rho}}$$
$$+\big(2\mathcal{L}_{31}(\hat{\rho})+\mathcal{L}_{32}(\hat{\rho})+\alpha(\hat{\rho})\mathcal{L}_{34}(\hat{\rho})\big)n_{\text{e}}(\hat{\rho},t)\frac{\partial T_{\text{e}}(\hat{\rho},t)}{\partial\hat{\rho}}\big], \tag{11}$$

where $\alpha(\hat{\rho})$, $\mathcal{L}_{31}(\hat{\rho})$, $\mathcal{L}_{32}(\hat{\rho})$ and $\mathcal{L}_{34}(\hat{\rho})$ are constant profiles which depend on the magnetic configuration of a particular plasma equilibrium.

The total injected power is expressed as $P_{\text{tot}}(t) = \sum_{i=1}^{i=N_{\text{NB}}} P_{\text{NB},i}(t)+P_{\text{EC}}(t)+P_{\text{ohm}}(t)-P_{\text{rad}}(t)$, where $P_{\text{ohm}}(t)$ is the ohmic heating power and $P_{\text{rad}}(t)$ is the radiated power. The ohmic heating power is given by $P_{\text{ohm}}(t) = \mathcal{R}_p(t)I_{\text{p}}(t)^2$, where $\mathcal{R}_p(t) = \int_0^1 \eta(\hat{\rho},t)\frac{dV}{d\hat{\rho}}d\hat{\rho}$ is the total plasma resistance and $V(\rho)$ is the volume enclosed by a magnetic surface within the plasma. The radiated power is modeled as $P_{\text{rad}}(t) = \int_0^1 Q_{\text{rad}}(\hat{\rho},t)\frac{dV}{d\hat{\rho}}d\hat{\rho}$, where $Q_{\text{rad}}(\hat{\rho},t) = k_{\text{brem}}Z_{\text{eff}}\,n_{\text{e}}(\hat{\rho},t)^2\sqrt{T_{\text{e}}(\hat{\rho},t)}$ and k_{brem} is the Bremsstrahlung radiation coefficient.

Using the control-oriented expressions (5), (6), (7), (8), (9), (10) and (11), equation (4) can be rewritten as

$$\frac{\partial\psi}{\partial t} = h_{diff}(\hat{\rho},t)\frac{\partial}{\partial\hat{\rho}}\left(\hat{\rho}D_\psi\frac{\partial\psi}{\partial\hat{\rho}}\right)+\sum_{i=1}^{N_{\text{NB}}}h_{\text{NB},i}(\hat{\rho},t)P_{\text{NB},i}(t)$$
$$+\,h_{\text{EC}}(\hat{\rho},t)P_{\text{EC}}(t)+h_{\text{BS}}(\hat{\rho},t)\left(\frac{\partial\psi}{\partial\hat{\rho}}\right)^{-1}, \tag{12}$$

where

$$h_{diff}(\hat{\rho},t) = \frac{\eta^{\text{prof}}(\hat{\rho})}{\mu_0\rho_b^2\hat{F}(\hat{\rho})\hat{\rho}}k_{diff}(t),$$
$$k_{diff}(t) = I_p^{-\frac{3}{2}\gamma}P_{\text{tot}}^{-\frac{3}{2}\epsilon}\bar{n}_{\text{e}}^{-\frac{3}{2}\zeta},$$
$$h_{\text{NB},i}(\hat{\rho},t) = R_0\eta^{\text{prof}}(\hat{\rho})\hat{H}(\hat{\rho})j_{\text{NB},i}^{\text{prof}}(\hat{\rho})\frac{\big(T_{\text{e}}^{\text{prof}}(\hat{\rho})\big)^{\delta_{\text{NB},i}}}{n_{\text{e}}^{\text{prof}}(\hat{\rho})}k_{\text{NB},i}(t),$$
$$k_{\text{NB},i}(t) = I_p^{\gamma(\delta_{\text{NB},i}-\frac{3}{2})}P_{\text{tot}}^{\epsilon(\delta_{\text{NB},i}-\frac{3}{2})}\bar{n}_{\text{e}}^{\zeta(\delta_{\text{NB},i}-\frac{3}{2})-1},$$
$$h_{\text{EC}}(\hat{\rho},t) = R_0\eta^{\text{prof}}(\hat{\rho})\hat{H}(\hat{\rho})j_{\text{EC}}^{\text{prof}}(\hat{\rho})\frac{\big(T_{\text{e}}^{\text{prof}}(\hat{\rho})\big)^{\delta_{\text{EC}}}}{n_{\text{e}}^{\text{prof}}(\hat{\rho})}k_{\text{EC}}(t),$$
$$k_{\text{EC}}(t) = I_p^{\gamma(\delta_{\text{EC}}-\frac{3}{2})}P_{\text{tot}}^{\epsilon(\delta_{\text{EC}}-\frac{3}{2})}\bar{n}_{\text{e}}^{\zeta(\delta_{\text{EC}}-\frac{3}{2})-1},$$
$$\eta^{\text{prof}}(\hat{\rho}) = \frac{k_{sp}^{\text{prof}}(\hat{\rho})Z_{\text{eff}}}{\big(T_{\text{e}}^{\text{prof}}(\hat{\rho})\big)^{3/2}\big(n_{\text{e}}^{\text{prof}}(\hat{\rho})\big)^{3\zeta/2}},$$
$$h_{\text{BS}}(\hat{\rho},t) = \frac{\eta^{\text{prof}}(\hat{\rho})k_{\text{JeV}}R_0^2\hat{H}(\hat{\rho})}{\hat{F}(\hat{\rho})}\big[2\mathcal{L}_{31}(\hat{\rho})T_{\text{e}}^{\text{prof}}(\hat{\rho})\frac{\partial n_{\text{e}}^{\text{prof}}}{\partial\hat{\rho}}$$
$$+\big(2\mathcal{L}_{31}(\hat{\rho})+\mathcal{L}_{32}(\hat{\rho})+\alpha(\hat{\rho})\mathcal{L}_{34}(\hat{\rho})\big)n_{\text{e}}^{\text{prof}}(\hat{\rho})\frac{\partial T_{\text{e}}^{\text{prof}}}{\partial\hat{\rho}}\big]k_{\text{BS}}(t),$$
$$k_{\text{BS}}(t) = I_p^{-\frac{1}{2}\gamma}P_{\text{tot}}^{-\frac{1}{2}\epsilon}\bar{n}_{\text{e}}^{-\frac{1}{2}\zeta+1},$$

where the time dependence in I_p, P_{tot} and $\bar{n}_{\text{e}}$ and the $\hat{\rho}$ dependence in the spatial derivatives of $T_{\text{e}}^{\text{prof}}$ and $n_{\text{e}}^{\text{prof}}$ have been dropped to ease the notation. The functions $h_{diff}(\hat{\rho},t)$, $h_{\text{NB},i}(\hat{\rho},t)$, $h_{\text{EC}}(\hat{\rho},t)$ and $h_{\text{BS}}(\hat{\rho},t)$ are determined from TRANSP data applicable to the scenario of interest. Therefore, in general, this model can be tailored to any tokamak scenario. In this work, the model is tailored to zero input-torque, reverse plasma-current ($I_{\text{p}} < 0$), high-confinement scenarios using data from DIII-D shots 163518 through 163525, in similar fashion as in [6].

III. Spatial Discretization and Linearization of the Central Safety Factor Model

The partial differential equation (12) is discretized in the $\hat{\rho}$-domain using finite differences to obtain a set of ordinary differential equations. A discretization grid with $N+1$ nodes in the interval $\hat{\rho} = [0,1]$ is used. The value of ψ at each of the nodes is denoted by ψ_j, for $j = 0,1,...,N$, and $\hat{\psi} = [\psi_0,\psi_1,...,\psi_N]^T$ is the state vector. After spatially discretizing (2) and (12), together with the boundary conditions (4), the model can be rewritten as

$$\dot{\hat{\psi}} = f\big(\hat{\psi},t,u(t)\big), \tag{13}$$
$$q_0 = g(\hat{\psi}), \tag{14}$$

where $f\big(\hat{\psi},t,u(t)\big)$ is a nonlinear function that describes the state evolution, $g(\hat{\psi})$ is a nonlinear function that describes the output evolution, and $u(t) = [P_{\text{NB},1}(t),...,P_{\text{NB},N_{\text{NB}}}(t),P_{\text{EC}}(t)]^T$ is the input vector. The control objective is to drive q_0 to a nominal trajectory $\bar{q}_0$. Linearizing with respect to a nominal trajectory of the system described by a state vector $\bar{\psi}(t)$ and an input vector $\bar{u}(t)$, it is possible to write (13), (14) and (2) as a linear, multi-input, single-output, time-varying system given by

$$\dot{\tilde{\psi}} = A(t)\tilde{\psi}+\sum_{i=1}^{i=N_{\text{NB}}}B_{1,i}(t)\tilde{P}_{\text{NB},i}(t)+B_2(t)\tilde{P}_{\text{EC}}(t), \tag{15}$$
$$\tilde{q}_0 = C(t)\tilde{\psi}, \tag{16}$$

where $\tilde{\psi} = \psi-\bar{\psi}$, $\tilde{u} = u-\bar{u}$, $\tilde{q}_0 = q_0-\bar{q}_0$, $A(t) \in \mathbb{R}^{(N+1)\times(N+1)}$ is the state matrix, $B_{1,i}(t) \in \mathbb{R}^{(N+1)\times 1}$ is the input matrix associated to the i-th NBI, $B_2(t) \in \mathbb{R}^{(N+1)\times 1}$ is the input matrix associated to the EC, and $C(t) \in \mathbb{R}^{1\times(N+1)}$ is the output matrix. These matrices are computed as $A(t) = \partial f\big(\hat{\psi},t,u(t)\big)/\partial\hat{\psi}$, $B_{1,i}(t) = \partial f\big(\hat{\psi},t,u(t)\big)/\partial P_{\text{NB},i}$ for $i = 1,...,N_{\text{NB}}$, $B_2(t) = \partial f\big(\hat{\psi},t,u(t)\big)/\partial P_{\text{EC}}$ and $C(t) = \partial g(\hat{\psi})/\partial\hat{\psi}$, all of them evaluated at $(\bar{\psi},\bar{u})$.

IV. Control Design

A. DIII-D Beams and Zero Input-Torque Condition

In the DIII-D tokamak, a total of 8 NBI's are available, i.e., $N_{\text{NB}} = 8$. These NBI's are denoted by 30L, 30R, 150L, 150R, 210L, 210R, 330L and 330R, and their configuration is depicted in Fig. 3. In this work, as a reverse plasma-current scenario is considered, 6 out of the 8 NBI's can drive current in the counter-current direction (30L, 30R, 150L, 150R, 330L and 330R), while 2 NBI's can drive current in the co-current direction (210L and 210R). The torque injected by a particular NBI is denoted as $T_{(\cdot)}$, where $(\cdot)$ is the designation of the NBI, i.e., $(\cdot) = 30L$, $(\cdot) = 30R$, etc. The total torque injected by the co-current NBI's is denoted by $T_{\text{NB},co}$, and it is given by

$$T_{\text{NB},co} = T_{210\text{L}} + T_{210\text{R}}. \tag{17}$$

The total torque injected by the counter-current NBI's is denoted by $T_{\text{NB},counter}$, and it is given by

$$T_{\text{NB},counter} = T_{30\text{L}} + T_{30\text{R}} + T_{150\text{L}} + T_{150\text{R}} + T_{330\text{L}} + T_{330\text{R}}. \tag{18}$$

The time dependence has been dropped in both (17) and (18) to ease notation. As a means to produce zero input-torque, the torque injected by the co-current NBI's must be equal to the torque injected by counter-current NBI's, i.e.,

$$T_{\text{NB},co} = T_{\text{NB},counter}. \tag{19}$$

In order to achieve condition (19), the NBI's are used in balanced groups. A balanced group is composed by one co-current NBI and one or more counter-current NBI's such that the co-current and counter-current torques are the same. Therefore, a balanced group injects zero input-torque. Two groups of paired NBI's are considered in this work: a first group composed by 30L, 150L, 330L and 210R, and a second group composed by 30R, 150R, 330R and 210L.

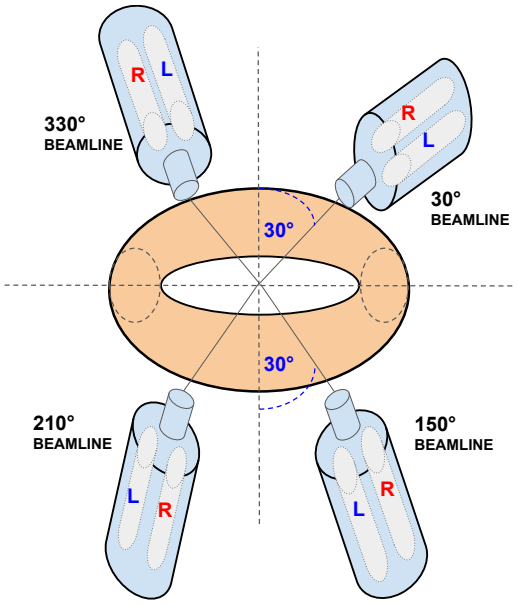

Fig. 3. Geometry and configuration of the NBI's in the DIII-D tokamak.

For any balanced group, the voltage of each NBI in DIII-D is adjusted according to their physical dimension and ion source so that the input-torque is close to zero if the power delivered to the co-current and counter-current NBI's is similar. Therefore, in terms of the power injected, the zero input-torque condition implies

$$P_{30\text{R}} + P_{150\text{R}} + P_{330\text{R}} = P_{210\text{L}}, \tag{20}$$

$$P_{30\text{L}} + P_{150\text{L}} + P_{330\text{L}} = P_{210\text{R}}, \tag{21}$$

where $P_{(\cdot)}$ is the power injected by the $(\cdot)$ NBI. In DIII-D, the maximum power that can be injected by each NBI is approximately 2 MW, i.e., $P_{\text{NB},i} \in [0, 2]$ MW, for $i = 1, ..., 8$. Also, the maximum EC power available is approximately 2 MW, i.e., $P_{\text{EC}} \in [0, 2]$ MW. In the DIII-D tokamak, the 150° beamline is physically smaller than the rest due to its capacity to inject particles off-axis, and also its ion source is different, so its voltage has to be higher than the other three beamlines in order to achieve the same torque. Keeping the 150° beamline with very high voltage for long time may damage it, so it is normally more convenient to use only the NBI's of the other three beamlines to produce zero input-torque.

Moreover, the total current density driven by each balanced group is small, because the current density contribution of the co-current NBI will mostly cancel out with the current density contribution of counter-current NBI's. The model substantially changes because there is no net current density driven by the NBI's, i.e., the second term on the right hand side of (12) is zero, $\sum_{i=1}^{N_{\text{NB}}} h_{\text{NB},i}(\hat{\rho}, t) P_{\text{NB},i}(t) = 0$. Each $P_{\text{NB},i}(t)$ only enters in (12) by affecting $P_{\text{tot}}(t)$ through the functions h_{diff}, h_{EC} and h_{BS}. Therefore, the relevant magnitude for NBI control is the total NBI power, instead of the individual powers of each NBI. The total NBI power is denoted as $P_{\text{NB}}(t) = \sum_{i=1}^{i=N_{\text{NB}}} P_{\text{NB},i}(t)$. With the previous arguments, equation (15) adopts a different shape given by

$$\dot{\tilde{\psi}} = A(t)\tilde{\psi} + B_1(t)\tilde{P}_{\text{NB}}(t) + B_2(t)\tilde{P}_{\text{EC}}(t), \tag{22}$$

where $B_1(t) \in \mathbb{R}^{(N+1)\times 1}$ is the time-varying input matrix associated to $\tilde{P}_{\text{NB}}(t)$. Then, the linearized system is still a multi-input, single-output system, but with 2 inputs instead of the $N_{\text{NB}} + 1$ that were considered before taking into account the zero input-torque condition.

B. PID Controller Design

As introduced above, the control objective is to drive q_0 to its nominal trajectory $\bar{q}_0$, or equivalently, $\tilde{q}_0$ to zero. Although (22) and (16) compose a time-varying system, the parameters of the PID controller are taken constant. The control laws for $\tilde{P}_{\text{NB}}$ and $\tilde{P}_{\text{EC}}$ are given by

$$\begin{bmatrix} \tilde{P}_{\text{NB}} \\ \tilde{P}_{\text{EC}} \end{bmatrix} = \begin{bmatrix} K_{p1} \\ K_{p2} \end{bmatrix} \tilde{q}_0 + \begin{bmatrix} 1/T_{i1} \\ 1/T_{i2} \end{bmatrix} \int_{t_0}^{t} \tilde{q}_0 dt + \begin{bmatrix} T_{d1} \\ T_{d2} \end{bmatrix} \frac{d\tilde{q}_0}{dt}, \tag{23}$$

where K_{p1}, T_{i1}, T_{d1}, K_{p2}, T_{i2} and T_{d2} are parameters that are designed to obtain a desired response of the closed-loop system, and t_0 is the initial time in which the error integral starts to be computed. Once that $P_{\text{NB}}(t) = \bar{P}_{\text{NB}}(t) + \tilde{P}_{\text{NB}}(t)$ is

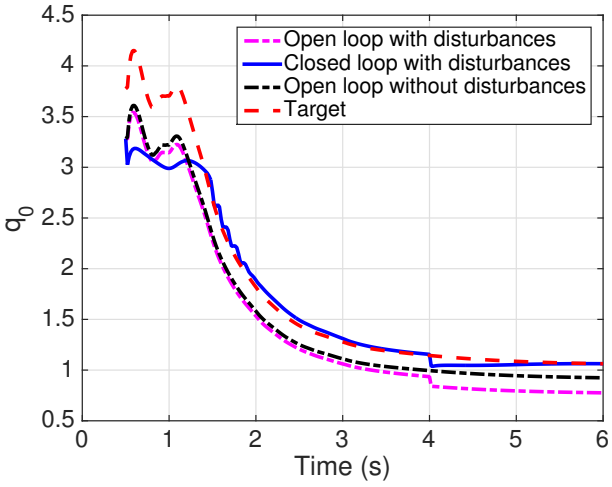

(a) Central safety factor q_0

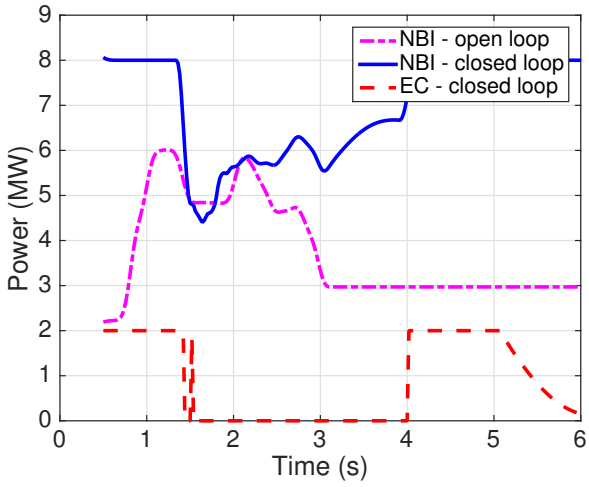

(b) P_{NB} and P_{EC}

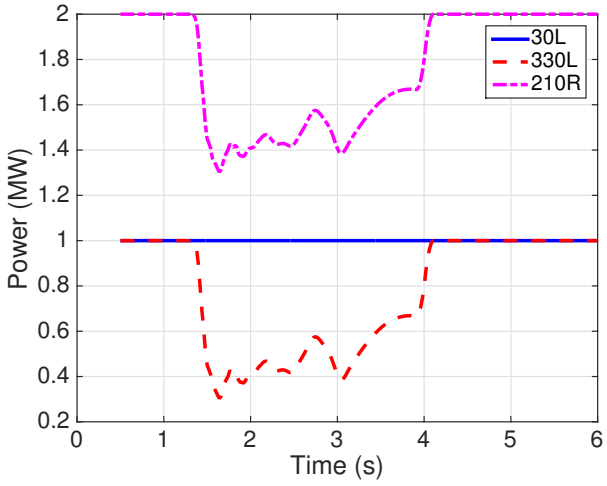

(c) $P_{\text{NB},i}$ of the 1st group

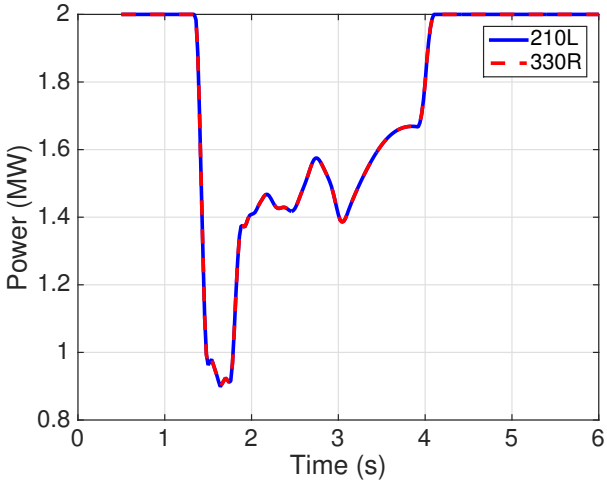

(d) $P_{\text{NB},i}$ of the 2nd group

Fig. 4. Simulation study: (a) q_0, (b) P_{NB} and P_{EC}, (c) NBI powers in closed loop for the 1^{st} balanced group, $P_{30\text{L}}$, $P_{330\text{L}}$ and $P_{210\text{R}}$, and (d) NBI powers in closed loop for the 2^{nd} balanced group, $P_{330\text{R}}$ and $P_{210\text{L}}$.

determined, $P_{\text{NB},i}(t)$ $(i = 1, ..., 8)$ is computed by using the zero input-torque condition given by (20)-(21). In general, there are 8 NBI's available, but the control law (23) and the zero-torque condition only impose three constraints, so five additional conditions/constraints must be specified in order to univocally determine $P_{\text{NB},i}(t)$ (i = 1, ..., 8) from $P_{\text{NB}}(t)$. Therefore, additional conditions must imposed on how the balanced group powers or individual NBI powers are set. Such conditions are determined based on the requirements of each particular scenario. An example which illustrates how conditions are imposed is shown in the simulation study of Section V.

V. Simulation Study

In this section, a simulation study is carried out to test the controller performance in a zero input-torque, high-confinement, reverse plasma-current ($I_p < 0$), DIII-D scenario. Although the controller is synthesized from a linear model, it is tested in a nonlinear simulation. The control-oriented model is tailored to DIII-D shots 163518 through 163525. Relevant machine parameters and experimental data for this scenario are $B_{\phi,0}$ = 1.93 T, R_0 = 1.69 m, Z_{eff} = 3.5, $\delta_{\text{NBI},i} = 0.5$, $\delta_{\text{EC}} = 1$, $\gamma = 1$, $\epsilon = 0.5$ and $\zeta = 0$. Moreover, the total available energy in the EC launchers during a shot is limited, and it may be convenient to use EC only in the most demanding situations. For such reason, EC is only used as a backup actuator in this simulation study, so if P_{NB} is not saturated, then $\tilde{P}_{\text{EC}}$ = 0. Therefore, the control law used in simulation is slightly different from (23), as it includes some logic to detect saturation of P_{NB} and set $\tilde{P}_{\text{EC}}$ = 0.

It is necessary to specify the additional conditions for the zero-input torque configuration. First, the 150° beamline is only used as a backup line due to its aforementioned special characteristics. Then, the controller sets $P_{150\text{L}} = P_{150\text{R}} = 0$ unless any of the other NBI fails, and extra power is needed to produce zero input-torque. Second, in order to obtain real-time q-profile reconstruction in DIII-D, it is necessary to keep $P_{30\text{L}} \geq 1$ MW. Then, it is chosen that the controller keeps $P_{30\text{L}} = 1$ MW, $\tilde{P}_{30\text{L}} = 0$. Third, the 30R NBI is not

used ($P_{30\text{R}} = 0$) to reproduce the conditions of shot 163520. Equations (20)-(21) become

$$1 \text{ MW} + P_{330\text{R}} = P_{210\text{L}}, \tag{24}$$

$$P_{330\text{L}} = P_{210\text{R}}. \tag{25}$$

Finally, it is imposed that each group of balanced NBI's injects the same amount of power, except if $\tilde{P}_{\text{NB}}$ as computed by the control law (23) is not high enough to ensure $P_{30\text{L}} = 1$ MW. In such case, all the power is injected by the first group of balanced beams (where 30L belongs to) in order to ensure q-profile reconstruction. All the introduced conditions allow for univocally determining $\tilde{P}_{\text{NB,i}}(t)$ (i = 1, ..., 8) once that $\tilde{P}_{\text{NB}}(t)$ has been determined from the control law (23).

In this simulation study, the controller attempts to regulate q_0 around a desired target $\bar{q}_0$ while rejecting external perturbations to the system. First, an open-loop simulation with the inputs P_{NB} and P_{EC} corresponding to the shot 163520 was executed, and a $\bar{q}_0^*$ evolution was obtained. Based on that $\bar{q}_0^*$ evolution, a new desired $\bar{q}_0$ evolution was computed. The target $\bar{q}_0$ is taken as $+15\%$ of the $\bar{q}_0^*$ evolution, i.e., $\bar{q}_0 = 1.15\bar{q}_0^*$. Such choice is based upon the requirement of $q_0 \geq 1$. Second, a closed-loop simulation with disturbances was executed in which the controller attempts to regulate q_0 around $\bar{q}_0$. A fictitious -20% decrease in j_{BS} is introduced during all the shot, representing some source of unknown variation in the bootstrap current density. Moreover, a constant -15% disturbance in q_0 is introduced between 4 s. and 6 s., emulating some unexpected MHD activity. Finally, an open-loop simulation with the previously described disturbances was executed.

Fig. 4(a) shows the q_0 evolution in open loop with disturbances (magenta dashed-dotted), in open loop without disturbances (black dashed-dotted), and in closed loop with disturbances (blue solid), together with the target $\bar{q}_0$ (red dashed). Fig. 4(b) shows the evolution of P_{NB} and P_{EC} for both open-loop and closed-loop simulations (note that P_{EC} is zero in open loop). Fig. 4(c) shows the evolution of the NBI powers in closed loop corresponding to the first balanced group, while Fig. 4(d) shows the evolution of the NBI power in closed loop corresponding to the second balanced group. As it can be seen in Fig. 4(a), from the initial time till 4 s., the open-loop simulation with disturbances shows that q_0 is smaller than in the open-loop simulation without disturbances, due to the reduction in j_{BS}. Also, the controller successfully drives q_0 to $\bar{q}_0$ in closed loop till 4s., when a sudden drop is suffered because of the constant q_0 disturbance introduced at that moment. After 4 s., the open-loop simulation with disturbances shows a constant drop in q_0, while the closed-loop simulation shows that the controller drives q_0 back to its reference value and is capable of keeping $q_0 \geq 1$, as desired. As it can be seen in Fig. 4(b), while P_{NB} is modulated by the controller during the whole shot, P_{EC} is only used as a backup actuator when P_{NB} is saturated between the beginning of the shot and ≈ 1.3 s (in order to achieve reference tracking), and between 4 s and ≈ 5.25 s (to recover from the sudden q_0 drop introduced as a disturbance).

VI. Summary and Future Work

A new controller is presented for the regulation of q_0 in tokamaks. Using linearization techniques, the nonlinear model of the q_0 evolution is transformed into a linear system for which a PID controller is designed. By means of a simulation study in a DIII-D scenario, it has been demonstrated this controller is able to drive the system to a distant target $\bar{q}_0$, and also that the controller is able to reject unknown perturbations to the system. Also, the simulation is executed in a high-confinement DIII-D scenario using realistic power and torque balance constraints that may be found in future tokamaks such as ITER.

Future work may include experimental testing of the controller in DIII-D adding an anti-windup compensator, or simulation testing for other scenarios different from DIII-D, as well as robustness studies of the control algorithm in presence of model uncertainties.

References

[1] J. Wesson, *Tokamaks*. Oxford, UK: Clarendon Press, 1984.

[2] J. Barton, M. Boyer, W. Shi, E. Schuster *et al.*, "Toroidal Current Profile Control During Low Confinement Mode Plasma Discharges in DIII-D via First-Principles-Driven Model-based Robust Control Synthesis," *Nuclear Fusion*, vol. 52, no. 123018, 2012.

[3] M. Boyer, J. Barton, E. Schuster *et al.*, "First-Principles-Driven Model-Based Current Profile Control for the DIII-D Tokamak via LQI Optimal Control," *Plasma Physics and Controlled Fusion*, vol. 55, no. 105007, 2013.

[4] M. Boyer, J. Barton, E. Schuster, M. Walker, T. Luce, J. Ferron, B. Penaflor, R. Johnson, and D. Humphreys, "Backstepping Control of the Toroidal Plasma Current Profile in the DIII-D Tokamak," *Control Systems Technology, IEEE Transactions on*, vol. 22, no. 5, pp. 1725–1739, Sept 2014.

[5] J. Barton, M. Boyer, E. Schuster *et al.*, "Physics-model-based nonlinear actuator trajectory optimization and safety factor profile feedback control for advanced scenario development in DIII-D," *Nucl. Fusion*, vol. 55, no. 093005, 2015.

[6] J. Barton, W. Shi *et al.*, "Physics-based Control-oriented Modeling of the Current Density Profile Dynamics in High-performance Tokamak Plasmas," *52nd IEEE International Conference on Decision and Control*, 2013.

[7] M. Boyer, R. Andre *et al.*, "Central safety factor and β_N control on NSTX-U via beam power and plasma boundary shape modification," *Nuclear Fusion*, vol. 55, 2015.

[8] Z. Ilhan, W. Wehner, J. Barton, E. Schuster, D. Gates, S. Gerhardt, and J. Menard, "First-Principles-Driven Model-Based Optimal Control of the Current Profile in NSTX-U," in *Proceedings of the 2015 IEEE Multi-conference on Systems and Control*, 2015.

[9] D. Moreau *et al.*, "A two-time-scale dynamic model approach for magnetic and kinetic profile control in advanced tokamak scenarios on JET," *Nuclear Fusion*, vol. 48, 2008.

[10] J. Barton, K. Besseghir, J. Lister, and E. Schuster, "Robust control of the safety factor profile and stored energy evolutions in high performance burning plasma scenarios in the ITER tokamak," *52nd IEEE Conference on Decision and Control*, pp. 4194–99, 2013.

[11] A. Garofalo, W. Salomon *et al.*, "Advances towards QH-mode viability for ELM-stable operation in ITER," *Nuclear Fusion*, vol. 51, p. 083018, 2011.

[12] PPPL. (2017) TRANSP homepage. [Online]. Available: http://w3.pppl.gov/transp/

[13] F. Hinton and R. Hazeltine, "Theory of plasma transport in toroidal confinement systems," *Rev. Mod. Phys.*, vol. 48, pp. 239–308, 1976.

[14] Y. Ou, T. Luce, E. Schuster *et al.*, "Towards model-based current profile control at DIII-D," *Fusion Engineering and Design*, vol. 82, pp. 1153–1160, 2007.

[15] O. Sauter *et al.*, "Neoclassical conductivity and bootstrap current formulas for general axisymmetric equilibria and arbitrary collisionality regime," *Physics of Plasmas*, vol. 6, no. 7, p. 2834, 1999.